Raman Spectroscopy Can Differentiate Malignant Tumors from Normal Breast Tissue and Detect Early Neoplastic Changes in a Mouse Model

Rachel E. Kast,[1] Gulay K. Serhatkulu,[2] Alex Cao,[2] Abhilash K. Pandya,[2] Houbei Dai,[1] Jagdish S. Thakur,[2] Vaman M. Naik,[3] Ratna Naik,[1] Michael D. Klein,[4] Gregory W. Auner,[2] Raja Rabah[5]

[1] *Department of Physics, Wayne State University, Detroit, MI*

[2] *Electrical and Computer Engineering Department, Wayne State University, Detroit, MI*

[3] *Department of Natural Sciences, University of Michigan-Dearborn, Dearborn, MI*

[4] *Department of Surgery (Pediatric Surgery), Wayne State University School of Medicine and Children's Hospital of Michigan, Detroit, MI*

[5] *Department of Pathology, Wayne State University School of Medicine and Children's Hospital of Michigan, Detroit, MI*

Received 12 July 2007; revised 7 November 2007; accepted 14 November 2007
Published online 26 November 2007 in Wiley InterScience (www.interscience.wiley.com). DOI 10.1002/bip.20899

ABSTRACT:

Raman spectroscopy shows potential in differentiating tumors from normal tissue. We used Raman spectroscopy with near-infrared light excitation to study normal breast tissue and tumors from 11 mice injected with a cancer cell line. Spectra were collected from 17 tumors, 18 samples of adjacent breast tissue and lymph nodes, and 17 tissue samples from the contralateral breast and its adjacent lymph nodes. Discriminant function analysis was used for classification with principal component analysis scores as input data. Tissues were examined by light microscopy following formalin fixation and hematoxylin and eosin staining. Discriminant function analysis and histology agreed on the diagnosis of all contralateral normal, tumor, and mastitis samples, except one tumor which was found to be more similar to normal tissue. Normal tissue adjacent to each tumor was examined as a separate data group called tumor bed. Scattered morphologically suspicious atypical cells not definite for tumor were present in the tumor bed samples. Classification of tumor bed tissue showed that some tumor bed tissues are diagnostically different from normal, tumor, and mastitis tissue. This may reflect malignant molecular alterations prior to morphologic changes, as expected in preneoplastic processes. Raman spectroscopy not only distinguishes tumor from normal breast tissue, but also detects early neoplastic changes prior to definite morphologic alteration. © *2007 Wiley Periodicals, Inc. Biopolymers 89: 235–241, 2008.*

Keywords: Raman spectroscopy; mouse model; cancer detection; pre-neoplastic changes; discriminant function analysis; histology

This article was originally published online as an accepted preprint. The "Published Online" date corresponds to the preprint version. You can request a copy of the preprint by emailing the Biopolymers editorial office at biopolymers@wiley.com

Correspondence to: Rachel Kast; e-mail: aw7315@wayne.edu
Contract grant sponsor: Wayne State University (President Reid Research Enhancement Program)

INTRODUCTION

Raman spectroscopy can provide details of the chemical composition of tissues. It is a nondestructive technique requiring no sample preparation, making it an attractive method for in vivo and in vitro characterization of biological tissues. A Raman spectrum

provides a molecular fingerprint, and the intensity of the Raman peaks is directly proportional to the concentration of the molecules. Traditional disease classification including cancer is based on the morphologic appearance of tissues (histology). These morphologic changes are accompanied by changes in chemical composition. Thus, Raman spectroscopy is likely to be a useful technique.[1–11]

The objectives of this study were to evaluate the sensitivity and specificity of Raman spectroscopy in differentiating between cancer and normal breast tissue in a mouse model.

MATERIALS AND METHODS

Animal Experiments

All experiments received prior approval from the Animal Investigation Committee at Wayne State University. A highly malignant BALB/c tumor cell line (4T1) was used in this study.[12] Eleven BALB/c (Taconic Farms, Germantown, NY) female mice (6- to 8-weeks old) were injected subcutaneously at the nipple of the 5th mammary gland on one side, with a suspension of 1×10^5 4T1 tumor cells. All mice developed tumor nodules at the injection site. The mice were humanely killed 10–14 days following injection. Tumors and adjacent breast tissue were removed for analysis. Adjacent breast tissue often included lymph nodes. The contralateral mammary gland and its adjacent lymph nodes were also removed. Specimens were evaluated histologically and with near-infrared (NIR) Raman spectroscopy. When lymph nodes were found histologically, they were also analyzed with Raman spectroscopy. Samples were divided in two. One was submitted for histology and one for Raman spectroscopy. After Raman spectroscopy, the samples used for Raman analysis were also submitted for histology.

Histology

Samples were fixed in 10% (v/v) neutral buffered zinc formalin solution (Richard Allan Scientific) and processed overnight. Following embedding, 5 μm sections were cut and stained with hematoxylin–eosin.

NIR Raman Spectroscopic Measurements

Raman spectra were recorded using a Renishaw Raman microscope (RM1000, equipped with a thermoelectric cooled 578 $\times$ 385 pixel CCD), using a 20$\times$ objective in the 600–1800 cm^{-1} spectral range. A 785 nm laser line was used to excite the Raman spectra with 50 mW of power at the sample. The spectra were collected in line-mode with a measured length and width of laser excitation of 130 μm $\times$ 25 μm. Typical cell size is on the order of 20 μm, and the line-mode was used to acquire spectra from a range of cells. This should be the preferred method in the operating room, as the surgeon would be unable to sample each cell individually because of limited cell selectivity and time constraints.

All Raman measurements used a 10 s exposure time, and three exposures were averaged to obtain a better signal-to-noise ratio. The spectral resolution was 4 cm^{-1}. To assess intrasample variability, multiple measurements ($n \geq 12$) were made on each sample at different regions. This was accomplished by placing samples on an *xyz* motorized, computer-controlled sample stage. Points to be analyzed were chosen randomly from the microscopic image of the tissue available on the Renishaw spectrometer.

Raman Spectrum Processing

Raman spectra of tissues contain a combination of Raman scattering, intrinsic tissue fluorescence, and noise. Preprocessing steps include cosmic-ray removal, noise subtraction, and removal of tissue fluorescence and normalization of the data. Each spectrum was represented as a set of 601 variables at 2 cm^{-1} intervals. A median filter was applied to the raw data to eliminate cosmic rays or spikes. Then noise was filtered using wavelets.[13] The background fluorescence was subtracted from the denoised spectra using a modified cubic spline algorithm. Unlike other cubic spline fits, this algorithm requires no a priori knowledge of the spectra.[14] The subtracted spectrum was normalized so that the minimum and maximum values of the spectrum were 0 and 1, respectively. Matlab version 6.5 was used to preprocess the data.

Tissue Classification Methods and Data Analysis

Principal component (PC) analysis was first used to reduce the dimensionality of the dataset to simplify the data analysis. Discriminant function analysis (DFA) was used for tissue classification. It is a supervised classification method that builds classification rules for a number of prespecified categories.[15] It correlates the weighting coefficients (scores) of the PCs calculated for each Raman spectrum with diagnostic categories. A leave-one-out classification algorithm was used to ensure the validity of the analysis.

RESULTS

Histological Evaluations

From the contralateral side, we collected normal breast tissue which often contained lymph nodes (Figure 1a). From the injected side, we collected tumor (Figure 1b), and adjacent breast tissue with lymph nodes (Figure 1c). We will refer to adjacent breast tissue with its accompanying lymph nodes as the tumor bed. Histology confirmed poorly differentiated adenocarcinoma in all 17 tumor samples. No definite tumor cells were found in any of the normal mammary tissue (tumor bed or contralateral), and no definite tumor cells were found in any of the lymph nodes from either side. The tumor bed samples showed reactive stromal cells, some inflammatory cells, and a few scattered large atypical cells with large hyperchromatic nuclei and a moderate amount of cytoplasm; however, they displayed no definite tumor aggregates (Figure 1c). In practice, atypical cells are hard to classify and are often overlooked. Two mice showed mastitis (fat necrosis and chronic inflammation) in their mammary gland tissue, one from tumor bed and two from contralateral breast (Figure 1d).

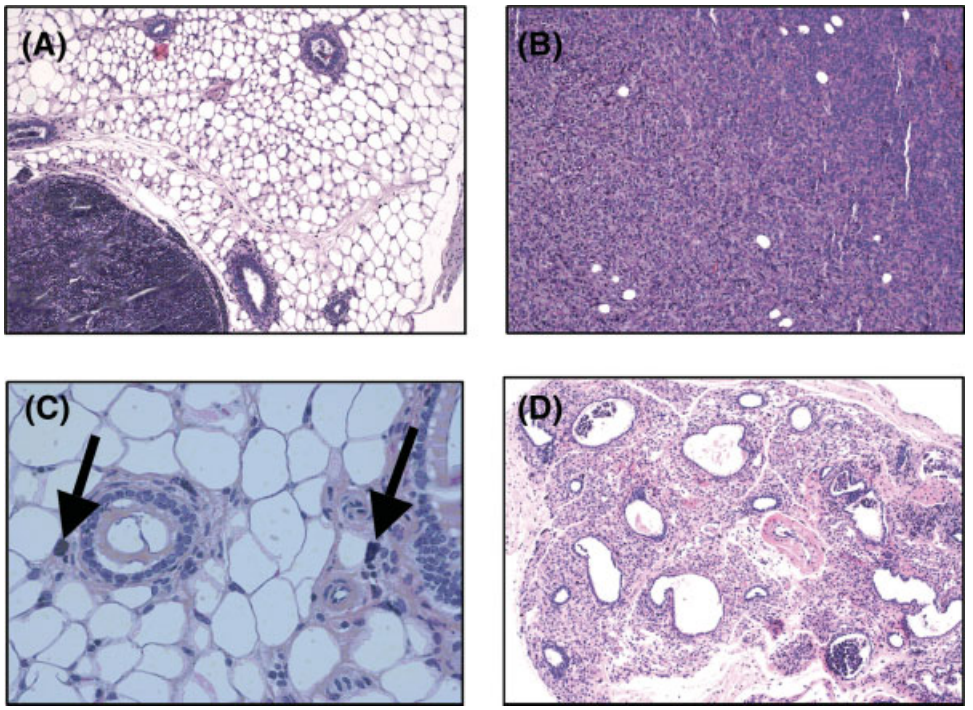

FIGURE 1 Histology images of typical (a) normal mammary gland with small benign lymph node seen in the left lower field, (b) tumor, (c) tumor bed (arrows point to atypical cells), and (d) mastitis.

Raman Spectroscopy

We collected 650 spectra. Because of the small size of the mammary glands and lymph nodes, we were not able to separate these tissues grossly. Some of the breast tissue samples contained tiny lymph nodes, and some of the lymph node samples contained breast tissue. For this reason, we analyzed the spectra in four diagnostic categories: (a) contralateral breast with lymph node, (b) tumor, (c) tumor bed, and (d) mastitis. Figure 2 shows the corresponding normalized mean Raman spectra. Note the visual differences in the peak heights of the four spectra.

Data Analysis

Mean Spectra Analysis. We first conducted an analysis of normal, tumor, and mastitis tissues to confirm the diagnostic ability of DFA. Raman and histology agreed in all cases, except one tumor sample which was more characteristic of normal tissue (Table I). This may be because the sample was largely made up of normal cells, with fewer tumor components.

We then analyzed the data using all four tissues—that is including tumor bed (Figure 2). These were also analyzed using DFA, with PC scores as the input using leave-one-out analysis. We used the mean spectra of each tissue to analyze the data, and then reanalyzed the data using individual spectra (Table II). Using mean spectra, 14 of 17 normal samples were correctly identified, 16 of 17 tumor samples were correctly identified, and all mastitis samples were correctly identified. Raman accuracy decreased slightly when including tumor bed, presumably because some tumor bed samples had characteristics of tumor while some had characteristics of normal tissue. Of 18 tumor bed samples, 9 were similar to the contralateral breast (normal), and 6 had specific changes separating them from normal tissue, 2 showed changes consistent with mastitis, and only 1 sample showed changes consistent with the other tumor samples. All mastitis samples were correctly identified.

Individual Spectra Analysis. Individual spectra also confirmed the ability of Raman to differentiate normal, tumor, and mastitis tissues. All normal and mastitis spectra were correctly identified, and 91% of tumor spectra were correctly identified. The other 9% were classified as normal and mastitis, consistent with normal pockets trapped within the tumor.

Using individual spectra, 79% of normal tissue samples were correctly identified, while the other 21% were identified as tumor bed. Within the tumor group, 0.4% were identified as normal, 10% were called tumor bed, 2.2% were called mastitis, and 87.3% were called tumor. All mastitis samples were correctly identified. Within the tumor bed, 49.2% of samples were identified as normal, 5.6% were identified as

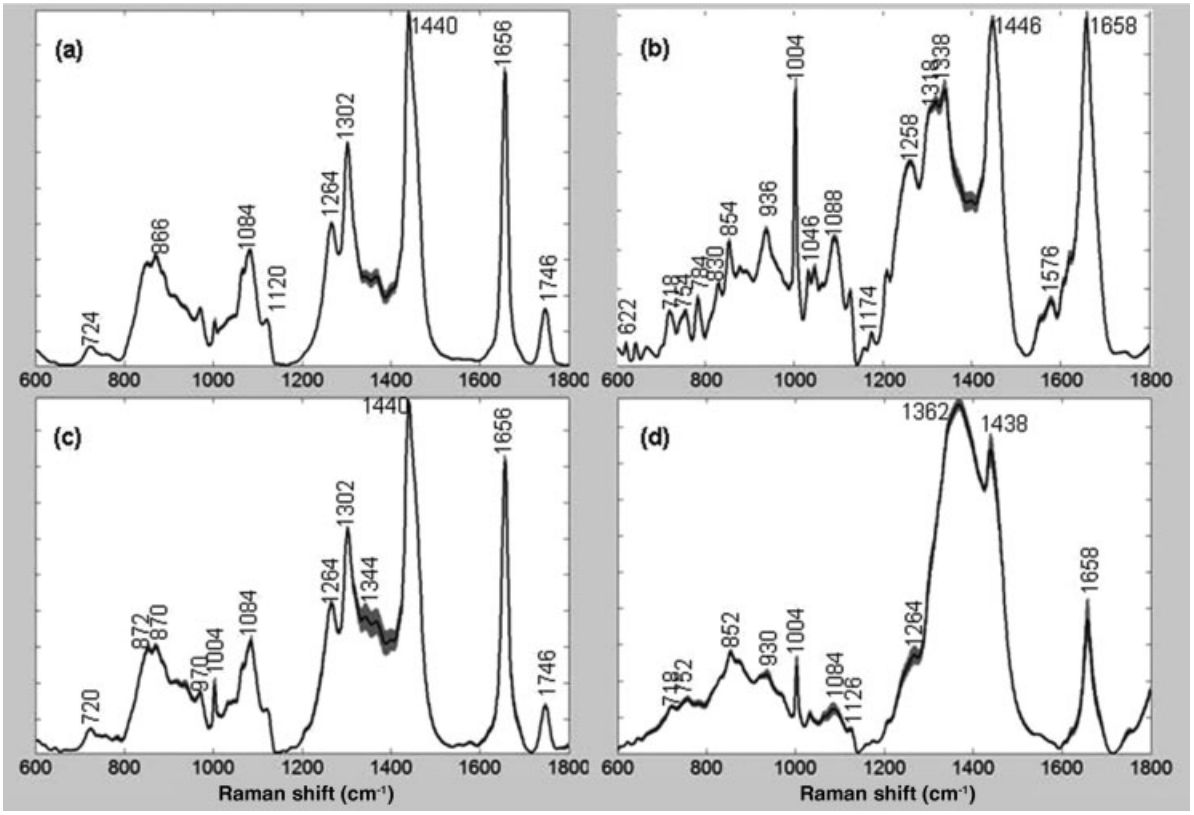

FIGURE 2 Mean Raman spectra of (a) normal mammary gland tissue with lymph nodes, (b) tumor, (c) tumor bed, and (d) mastitis. The gray region designates the 95% confidence interval for each peak.

Table I Leave-One-Out DFA Classification Results Using Three Data Groups

	Mean Spectra Analysis (*n*)				Casewise Analysis (*n*)			
Tissue Type	Samples	Normal	Tumor	Mastitis	Samples	Normal	Tumor	Mastitis
Normal	17	17			189	189		
Tumor	17	1	16		229	15	209	5
Mastitis	3			3	37			37

The number in each column represents the number of cases per group as classified by the diagnostic method.

Table II Leave-One-Out Results of DFA for Tumor Bed Analysis

	Mean Spectra Analysis (*n*)					Casewise Analysis (*n*)				
Tissue Type	Samples	Normal	Tumor	Mastitis	Tumor Bed	Samples	Normal	Tumor	Mastitis	Tumor Bed
Normal	17	14			3	189	150			39
Tumor	17		16		1	229	1	200	5	23
Mastitis	3			3		37			37	
Tumor bed	18	9	1	2	6	195	96	11	10	78

The number in each column represents the number of cases per group as classified by the diagnostic method.

Table III Tentative Peak Assignments

Normal Mam. Gland	Tumor	Mastitis	Tumor Bed	Assignment
	622			C—C twisting mode of phenylalanine[16–18]
	642			C—C twist of tyrosine[16,18]
	666		664	T ,G and ν(C—S) of cysteine (DNA/RNA)[17,18]
724	718	718	720	C—N (membrane phospholipid head)/nucleotide peak symmetric choline stretch, phospholipids, (H3C)N+ stretch band[16,19–21]
	754	752		Symmetric breathing of tryptophan[18]
762			758	Symmetric ring breathing of tryptophan, ν_s(O—P—O)[16,17,19,22]
	784		782	U,C,T ring breathing, DNA[17]
	830			Out-of-plane ring breathing tyrosine/ν(O—P—O), DNA[16]
	854	852	852	Ring breathing of tyrosine and ν(C—C) hydroxyproline ring specific to collagen[16,17,19]
868			870	Proline[18]
	876			ν(C—C), hydroxyproline[11]
	936			ν(C—C) protein backbone α-helix (proline/glycogen), collagen[16,17,19,20,23,24]
968			970	δ(=CH) wagging[3]
1004	1004	1002	1004	ν_S symmetric ring breathing mode, phenylalanine[16,17,19,24]
		1032		δ (C—H), phenylalanine[16]
	1046			C—O stretching of carbohydrates[17]
1084	1088	1084	1084	C—N stretching of proteins and lipids, ν(C—C) and ν(C—O) of phospholipids[17,18,25]
1120	1126	1126		ν(C—C)of lipids from trans—segments and ν(C—N)of proteins[24]
	1174			δ(C—H), tyrosine[16]
	1258			Amide III, β-sheet/adenine and cytosine[16,17,20]
1264		1264	1264	δ(=CH)of lipids[11,16,17,20,24]
1302			1302	(CH_2) twist, phospholipids and collagen[17,25]
	1318			Guanine, CH_3CH_2 wagging nucleic acids, CH_3CH_2 wagging collagen[11,17]
	1338			Amide III, hydrated α-helix δ(N—H) and ν(C—N), desmosine/isodesmosine(elastin) (A and G of DNA/RNA)[16,17,19,26]
			1344	A and G of DNA/RNA and CH deformation of proteins[27]
1364		1362	1366	Guaninine, TRP (protein), lipids[18]
1440	1446	1438	1440	δ (CH_2) δ as (CH_3) in proteins (around 1449) and lipids (around 1438)[19,20,24,28]
	1576		1574	Tryptophan, Nucleic acids(guanine, adenine) TRP protein[16,20,28]
1656	1658	1658	1656	(Amide I, α-helix) , υ(C=O) of proteins collagen, elastin and ν(C=C) of lipids(around 1654 cm^{-1})[17,18,26]
1746			1746	ν(C=O) of phospholipids[11,19,29]

ν, stretching mode; ν_s, symmetric stretch; ν_{as}, asymmetric stretch; δ, bending mode.

tumor, 5.1% were identified as mastitis, and 40% were accurately called tumor bed.

DISCUSSION

Several literature sources identify specific molecular structures with specific Raman peaks. The relevant peak assignments for our data are noted in Table III. The Raman spectrum of normal mammary gland and associated lymph nodes (Figure 2a) is dominated by contribution from lipids. The peaks at 1004, 868, and 762 cm^{-1} reflect the protein-rich composition of the tissue.

The Raman spectra of mammary gland tumors (Figure 2b) reflect increased protein and reduced lipid compared to normal mammary gland tissue. This is demonstrated by (i) decreased intensity of the 1746 cm^{-1} peak due to C=O stretch of phospholipids, (ii) the decreased intensity of the 1440 cm^{-1}, and (iii) new or more intense protein peaks around 1576, 1446, 1338, 1318, 1258, 1174, 1004, 936, 854, 830, 642, and 622 cm^{-1}.

The spectral profile of tumor bed (Figure 2c) produced the same peaks as normal mammary gland tissue, with some slight changes in the peak intensities.

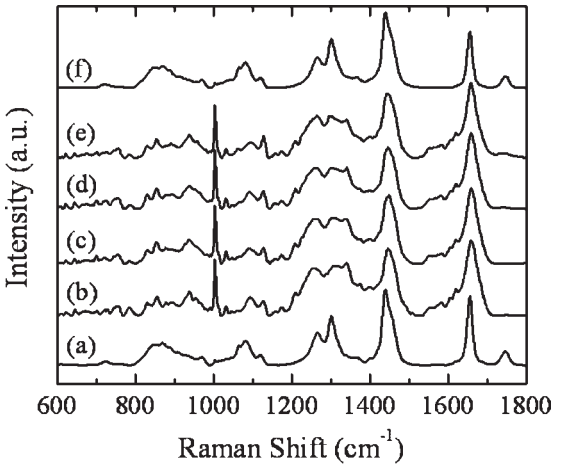

FIGURE 3 Raman mapping studies. Two different Raman spectral profiles are obtained, traces labeled scans b, c, d, and e are compatible with Raman spectral profile of a tumor, whereas the traces labeled a and f are similar to the spectral profiles of normal mammary gland.

Mastitis is characterized by destruction of mature adipose tissue with sheets of inflammatory cells and foamy macrophages. Raman spectra of mastitis (Figure 2d) lacked the phospholipid peak at 1747 cm^{-1} and showed superimposed peaks in the 1200–1500 cm^{-1} region, resulting in a noticeably broad spectral feature.

Other studies have also shown the ability of Raman spectroscopy to accurately classify diseased tissue in brain,[16,17] skin,[18–24] cervix,[25–27] breast,[1,2,9,10,28–33] and other organs.[8,11,34–44] Our data is confirmatory, and, in addition, demonstrates changes in the tumor bed, which probably represent the detection of chemical signs of preneoplastic changes.

Not every Raman spectra correctly classifies every tissue sample. The reason that some spectra from a sample are different is that all samples contain a variety of tissues, such as blood vessels, residual normal organ tissue, and fat.[25,26] For example, Figure 3 shows the Raman spectra of six different points on the same tumor sample. There are clear differences in the spectral (and therefore chemical) compositions between points b, c, d, e, and a and f, which may reflect two trapped normal components within a tumor sample. Even tumor samples can be expected to contain normal blood vessels and fat. Thus, it would not be a rare event for the Raman microscope to interrogate normal tissue within the tumor. For this reason we take at least 12 spectra from each sample and eliminate the obviously aberrant spectra. We then decide on the diagnosis using the average of all spectra obtained from that sample. Our results firmly support the ability of Raman spectra, when appropriately averaged, preprocessed, and analyzed, to reach the same diagnostic conclusions as histology.

While these results are promising, they may misconstrue the actual diagnostic ability of Raman spectroscopy. All spectra were collected under controlled conditions with little intersample variability, under the supervision of trained pathologists. In a less-controlled in vivo study, the diagnostic ability may be reduced because of increased variability in collection method and less premeasurement knowledge of the sample.

In clinical practice, malignant tumors are usually excised with a significant amount of surrounding normal tissue to guarantee complete removal of atypical and preneoplastic cells. Raman spectroscopy indicates that surrounding normal tissue is not the same as the contralateral normal breast. Most of the "errors" that were made were in classification of the tumor bed. Some tumor bed tissues were distinctly different from normal, tumor, and mastitis tissues. This may reflect malignant molecular alterations prior to morphologic changes, as would be expected in preneoplastic processes.

Before Raman can be translated to in vivo use, many barriers must be overcome. A new system should be designed, which can be integrated into an existing surgical tool, such as an endoscope or needle biopsy system. To meet this challenge, a fiber-optic probe must be designed, which can be inserted into the needle or endoscope. Ideally, the fiber would reduce the collection time to fractions of a second while also reducing fluorescence. Accompanying software must preprocess and classify the data in near real-time to give an immediate diagnosis in the operating room.

Our study demonstrates that tissues have characteristic Raman spectral features that differentiate pathologic changes like mastitis and cancer from normal breast tissue in a mouse model. It also suggests that Raman spectroscopy can detect molecular preneoplastic changes prior to histologic alterations. This is a rapid technique and requires no prior preparation of tissue. Tissue can be examined in vitro or in vivo in seconds, and if a library of spectral profiles of various tissues and pathologic conditions is created, comparison and interpretation can be performed in real-time. It may offer a quicker, less-subjective method to detect cancer as a supplement to current histological methods. With the rapid development and improvement of optic and computer technology, fiber-optic Raman probes may be used by clinicians to detect malignancy and by surgeons to guide surgical excisions in the not very distant future.

The authors thank Children's Hospital of Michigan, Detroit, MI, for partially funding this effort.

REFERENCES

1. Haka, A. S.; Volynskaya, Z.; Gardecki, J. A.; Nazemi, J.; Lyons, J.; Hicks, D.; Fitzmaurice, M.; Dasari, R. R.; Crowe, J. P.; Feld, M. S. Cancer Res 2006, 66, 3317–3322.

2. Haka, A. S.; Shafer-Peltier, K. E.; Fitzmaurice, M.; Crowe, J.; Dasari, R. R.; Feld, M. S. Proc Natl Acad Sci USA 2005, 102, 12371–12376.
3. Lakshmi, J. Radiat Res 2002, 157, 175–182.
4. Shim, M. G.; Wong Kee Song, L.-M., Marcon, N. E.; Wilson, B. C. Photochem Photobiol 2000, 72, 146–150.
5. Schut, T. C. B.; Witjes, M. J. H.; Sterenborg, H. J. C. M.; Speelman, O. C.; Roodenburg, J. L. N.; Marple, E. T.; Bruining, H. A.; Puppels, G. J. Anal Chem 2000, 72, 6010–6018.
6. Puppels, G. J.; Schut, T. C. B.; Caspers, P. J.; Wolthuis, R.; van Aken, M.; van der Laarse, A.; Bruining, H. A.; Buschmann, H. P. J.; Shim, M. G.; Wilson, B. C. Pract Spectrosc 2001, 28, 540–574.
7. Manoharan, R.; Wang, Y.; Boustany, N.; Brennan, J. F.; Baraga, J. J.; Dasari, R. R.; Van Dam, J.; Singer, S.; Feld, M. S. Proc SPIE-Int Soc Opt Eng 1994, 2328, 128–132.
8. Kaminaka, S.; Yamazaki, H.; Ito, T.; Kohda, E.; Hamaguchi, H.-O. J Raman Spectrosc 2001, 32, 139–141.
9. Frank, C. J.; Redd, D. C.; Gansler, T. S.; McCreery, R. L. Anal Chem Feb 1 1994, 66(3):319–326.
10. Frank, C. J.; McCreery, R. L.; Redd, D. C. Anal Chem 1995, 67, 777–783.
11. Huang, Z.; McWilliams, A.; Lui, H.; McLean, D. I.; Lam, S.; Zeng, H. Int J Cancer 2003, 107, 1047–1052.
12. Aslakson, C. J.; Miller, F. R. Cancer Res 1992, 52, 1399–1405.
13. Cai, T. T.; Zhang, D.; Ben-Amotz, D. Appl Spectrosc 2001, 55, 1124–1130.
14. Thakur, J. G.; Dai, H.; Serhatkulu, G. K.; Naik, R.; Naik, V. M.; Cao, A.; Pandya, A.; Auner, G. W.; Rabah, R.; Klein, M. D.; Freeman, C. J Raman Spectrosc 2007, 38, 127–134.
15. Tormod, N.; Isaksson, T.; Fearn, T.; Davies, T. A User Friendly Guide to Multivariate Calibration and Classification; NIR Publications: Chichester, UK, 2002.
16. Krafft, C.; Miljanic, S.; Sobottka, S. B.; Schackert, G.; Salzer, R. Proc SPIE-Int Soc Opt Eng 2003, 5141, 230–236.
17. Wolthuis, R.; van Aken, M.; Fountas, K.; Robinson, J. S., Jr.; Bruining, H. A.; Puppels, G. J. Anal Chem 2001, 73, 3915–3920.
18. Fendel, S.; Schrader, B. Fresenius' J Anal Chem 1998, 360, 609–613.
19. Gniadecka, M.; Philipsen Peter, A.; Sigurdsson, S.; Wessel, S.; Nielsen Ole, F.; Christensen Daniel, H.; Hercogova, J.; Rossen, K.; Thomsen Henrik, K.; Gniadecki, R.; Hansen Lars, K.; Wulf Hans, C. J Invest Dermatol 2004, 122, 443–449.
20. Gniadecka, M.; Wulf, H. C.; Mortensen, N. N.; Nielsen, O. F.; Christensen, D. H. J Raman Spectrosc 1997, 28, 125–129.
21. Gniadecka, M.; Wulf, H. C.; Nielsen, O. F.; Christensen, D. H.; Hercogova, J. Photochem Photobiol 1997, 66, 418–423.
22. Gniadecka, M.; Wulf, H. C.; Nielsen, O. F.; Christensen, D. H.; Hercogova, J. Spectrosc Biol Mol: Modern Trends (Seventh European Conference on Spectroscopy of Biological Molecules, Madrid, 1997) 1997, 449–450.
23. Hata, T. R.; Scholz, T. A.; Ermakov, I. V.; McClane, R. W.; Khachik, F.; Gellermann, W.; Pershing, L. K. J Invest Dermatol 2000, 115, 441–448.
24. Johansson, C. K.; Christensen, D. H.; Nielsen, O. F. Dansk Kemi 1999, 80, 12–13.
25. Mahadevan-Jansen, A.; Mitchell, M. F.; Ramanujam, N.; Malpica, A.; Thomsen, S.; Utzinger, U.; Richards-Kortum, R. Photochem Photobiol 1998, 68, 123–132.
26. Mahadevan-Jansen, A.; Robichaux, A.; Lieber, C.; Shappell, H.; Ellis, D.; Jones, H. W., III. Trends Opt Photon 2002, 71, 345–348.
27. Utzinger, U.; Heintzelman, D. L.; Mahadevan-Jansen, A.; Malpica, A.; Follen, M.; Richards-Kortum, R. Appl Spectrosc 2001, 55, 955–959.
28. Frank, C. J.; McCreery, R. L.; Redd, D. C. B. Anal Chem 1995, 67, 777–783.
29. Frank, C. J.; Redd, D. C.; Gansler, T. S.; McCreery, R. L. Anal Chem 1994, 66, 319–326.
30. Haka, A. S.; Shafer-Peltier, K. E.; Fitzmaurice, M.; Crowe, J.; Dasari, R. R.; Feld, M. S. Trends Opt Photon 2002, 71, 349–351.
31. Haka, A. S.; Shafer-Peltier, K. E.; Fitzmaurice, M.; Crowe, J.; Dasari, R. R.; Feld, M. S. Cancer Res 2002, 62, 5375–5380.
32. Manoharan, R.; Shafer, K.; Perelman, L.; Wu, J.; Chen, K.; Deinum, G.; Fitzmaurice, M.; Myles, J.; Crowe, J.; Dasari, R. R.; Feld, M. S. Photochem Photobiol 1998, 67, 15–22.
33. Redd, D. C. B.; Feng, Z. C.; Yue, K. T.; Gansler, T. S. Appl Spectrosc 1993, 47, 787–791.
34. Molckovsky, A.; Song, L. M.; Shim, M. G.; Marcon, N. E.; Wilson, B. C. Gastrointest Endosc 2003, 57, 396–402.
35. Stone, N.; Kendall, C.; Shepherd, N.; Crow, P.; Barr, H. J Raman Spectrosc 2002, 33, 564–573.
36. Stone, N.; Kendall, C.; Smith, J.; Crow, P.; Barr, H. Faraday Discuss 2003, 126, 141–157.
37. Stone, N.; Stavroulaki, P.; Kendall, C.; Birchall, M.; Barr, H. Laryngoscope 2000, 110, 1756–1763.
38. Venkatakrishna, K.; Kurien, J.; Pai, K. M.; Valiathan, M.; Kumar, N. N.; Krishna, C. M.; Ullas, G.; Kartha, V. B. Curr Sci 2001, 80, 665–669.
39. Malini, R.; Venkatakrishna, K.; Kurien, J.; Pai, K. M.; Rao, L.; Kartha, V. B.; Krishna, C. M. Biopolymers 2006, 81, 179–193.
40. Wu, J. G.; Xu, Y. Z.; Sun, C. W.; Soloway, R. D.; Xu, D. F.; Wu, Q. G.; Sun, K. H.; Weng, S. F.; Xu, G. X. Biopolymers 2001, 62, 185–192.
41. Crow, P.; Barrass, B.; Kendall, C.; Hart-Prieto, M.; Wright, M.; Persad, R.; Stone, N. Br J Cancer 2005, 92, 2166–2170.
42. Crow, P.; Stone, N.; Kendall, C. A.; Uff, J. S.; Farmer, J. A.; Barr, H.; Wright, M. P. Br J Cancer 2003, 89, 106–108.
43. Crow, P.; Uff, J. S.; Farmer, J. A.; Wright, M. P.; Stone, N. BJU Int 2004, 93, 1232–1236.
44. Nayak, G. S.; Kamath, S.; Pai, K. M.; Sarkar, A.; Ray, S.; Kurien, J.; D'Almeida, L.; Krishnananand, B. R.; Santhosh, C.; Kartha, V. B.; Mahato, K. K. Biopolymers 2006, 82, 152–166.

Reviewing Editor: Laurence Nafie